

Measurement of $|V_{cb}|$ using $\bar{B}^0 \rightarrow D^{*+} \ell^- \bar{\nu}$ decays

The OPAL Collaboration

Abstract

The magnitude of the Cabibbo-Kobayashi-Maskawa matrix element V_{cb} has been measured using $\bar{B}^0 \rightarrow D^{*+} \ell^- \bar{\nu}$ decays recorded on the Z^0 peak using the OPAL detector at LEP. The $D^{*+} \rightarrow D^0 \pi^+$ decays were reconstructed both in the particular decay modes $D^0 \rightarrow K^- \pi^+$ and $D^0 \rightarrow K^- \pi^+ \pi^0$ and via an inclusive technique. The product of $|V_{cb}|$ and the decay form factor of the $\bar{B}^0 \rightarrow D^{*+} \ell^- \bar{\nu}$ transition at zero recoil $\mathcal{F}(1)$ was measured to be $\mathcal{F}(1)|V_{cb}| = (37.1 \pm 1.0 \pm 2.0) \times 10^{-3}$, where the uncertainties are statistical and systematic respectively. By using Heavy Quark Effective Theory calculations for $\mathcal{F}(1)$, a value of

$$|V_{cb}| = (40.7 \pm 1.1 \pm 2.2 \pm 1.6) \times 10^{-3}$$

was obtained, where the third error is due to theoretical uncertainties in the value of $\mathcal{F}(1)$. The branching ratio $\text{Br}(\bar{B}^0 \rightarrow D^{*+} \ell^- \bar{\nu})$ was also measured to be $(5.26 \pm 0.20 \pm 0.46)\%$.

Submitted to Physics Letters B.

The OPAL Collaboration

G. Abbiendi², K. Ackerstaff⁸, P.F. Akesson³, G. Alexander²², J. Allison¹⁶, K.J. Anderson⁹, S. Arcelli¹⁷,
 S. Asai²³, S.F. Ashby¹, D. Axen²⁷, G. Azuelos^{18,a}, I. Bailey²⁶, A.H. Ball⁸, E. Barberio⁸, R.J. Barlow¹⁶,
 J.R. Batley⁵, S. Baumann³, T. Behnke²⁵, K.W. Bell²⁰, G. Bella²², A. Bellerive⁹, S. Bentvelsen⁸,
 S. Bethke^{14,i}, O. Biebel^{14,i}, A. Biguzzi⁵, I.J. Bloodworth¹, P. Bock¹¹, J. Böhme^{14,h}, O. Boeriu¹⁰,
 D. Bonacorsi², M. Boutemur³¹, S. Braibant⁸, P. Bright-Thomas¹, L. Brigliadori², R.M. Brown²⁰,
 H.J. Burckhart⁸, J. Cammin³, P. Capiluppi², R.K. Carnegie⁶, A.A. Carter¹³, J.R. Carter⁵,
 C.Y. Chang¹⁷, D.G. Charlton^{1,b}, D. Chrisman⁴, C. Ciocca², P.E.L. Clarke¹⁵, E. Clay¹⁵, I. Cohen²²,
 O.C. Cooke⁸, J. Couchman¹⁵, C. Couyoumtzelis¹³, R.L. Coxe⁹, M. Cuffiani², S. Dado²¹,
 G.M. Dallavalle², S. Dallison¹⁶, R. Davis²⁸, A. de Roeck⁸, P. Dervan¹⁵, K. Desch²⁵, B. Dienes^{30,h},
 M.S. Dixit⁷, M. Donkers⁶, J. Dubbert³¹, E. Duchovni²⁴, G. Duckeck³¹, I.P. Duerdoth¹⁶,
 P.G. Estabrooks⁶, E. Etzion²², F. Fabbri², A. Fanfani², M. Fanti², A.A. Faust²⁸, L. Feld¹⁰, P. Ferrari¹²,
 F. Fiedler²⁵, M. Fierro², I. Fleck¹⁰, A. Frey⁸, A. Fürties⁸, D.I. Futyan¹⁶, P. Gagnon¹², J.W. Gary⁴,
 G. Gaycken²⁵, C. Geich-Gimbel³, G. Giacomelli², P. Giacomelli², D.M. Gingrich^{28,a}, D. Glenzinski⁹,
 J. Goldberg²¹, W. Gorn⁴, C. Grandi², K. Graham²⁶, E. Gross²⁴, J. Grunhaus²², M. Gruwe²⁵,
 P.O. Günther³, C. Hajdu²⁹, G.G. Hanson¹², M. Hansroul⁸, M. Hapke¹³, K. Harder²⁵, A. Harel²¹,
 C.K. Hargrove⁷, M. Harin-Dirac⁴, A. Hauke³, M. Hauschild⁸, C.M. Hawkes¹, R. Hawkings²⁵,
 R.J. Hemingway⁶, C. Hensel²⁵, G. Herten¹⁰, R.D. Heuer²⁵, M.D. Hildreth⁸, J.C. Hill⁵, P.R. Hobson²⁵,
 A. Hocker⁹, K. Hoffman⁸, R.J. Homer¹, A.K. Honma⁸, D. Horváth^{29,c}, K.R. Hossain²⁸, R. Howard²⁷,
 P. Hüntemeyer²⁵, P. Igo-Kemenes¹¹, D.C. Imrie²⁵, K. Ishii²³, F.R. Jacob²⁰, A. Jawahery¹⁷,
 H. Jeremie¹⁸, M. Jimack¹, C.R. Jones⁵, P. Jovanovic¹, T.R. Junk⁶, N. Kanaya²³, J. Kanzaki²³,
 G. Karapetian¹⁸, D. Karlen⁶, V. Kartvelishvili¹⁶, K. Kawagoe²³, T. Kawamoto²³, P.I. Kayal²⁸,
 R.K. Keeler²⁶, R.G. Kellogg¹⁷, B.W. Kennedy²⁰, D.H. Kim¹⁹, K. Klein¹¹, A. Klier²⁴, T. Kobayashi²³,
 M. Kobel³, T.P. Kokott³, M. Kolrep¹⁰, S. Komamiya²³, R.V. Kowalewski²⁶, T. Kress⁴, P. Krieger⁶,
 J. von Krogh¹¹, T. Kuhl³, M. Kupper²⁴, P. Kyberd¹³, G.D. Lafferty¹⁶, H. Landsman²¹, D. Lanske¹⁴,
 I. Lawson²⁶, J.G. Layter⁴, A. Leins³¹, D. Lellouch²⁴, J. Letts¹², L. Levinson²⁴, R. Liebisch¹¹,
 J. Lillich¹⁰, B. List⁸, C. Littlewood⁵, A.W. Lloyd¹, S.L. Lloyd¹³, F.K. Loebinger¹⁶, G.D. Long²⁶,
 M.J. Losty⁷, J. Lu²⁷, J. Ludwig¹⁰, A. Macchiolo¹⁸, A. Macpherson²⁸, W. Mader³, M. Mannelli⁸,
 S. Marcellini², T.E. Marchant¹⁶, A.J. Martin¹³, J.P. Martin¹⁸, G. Martinez¹⁷, T. Mashimo²³,
 P. Mättig²⁴, W.J. McDonald²⁸, J. McKenna²⁷, T.J. McMahon¹, R.A. McPherson²⁶, F. Meijers⁸,
 P. Mendez-Lorenzo³¹, F.S. Merritt⁹, H. Mes⁷, I. Meyer⁵, A. Michelini², S. Mihara²³, G. Mikenberg²⁴,
 D.J. Miller¹⁵, W. Mohr¹⁰, A. Montanari², T. Mori²³, K. Nagai⁸, I. Nakamura²³, H.A. Neal^{12,f},
 R. Nisius⁸, S.W. O'Neale¹, F.G. Oakham⁷, F. Odoric², H.O. Ogren¹², A. Okpara¹¹, M.J. Oreglia⁹,
 S. Orito²³, G. Pásztor²⁹, J.R. Pater¹⁶, G.N. Patrick²⁰, J. Patt¹⁰, R. Perez-Ochoa⁸,
 P. Pfeifenschneider¹⁴, J.E. Pilcher⁹, J. Pinfold²⁸, D.E. Plane⁸, B. Poli², J. Polok⁸, M. Przybycień^{8,d},
 A. Quadt⁸, C. Rembser⁸, H. Rick⁸, S.A. Robins²¹, N. Rodning²⁸, J.M. Roney²⁶, S. Rosati³,
 K. Roscoe¹⁶, A.M. Rossi², Y. Rozen²¹, K. Runge¹⁰, O. Runolfsson⁸, D.R. Rust¹², K. Sachs¹⁰,
 T. Saeki²³, O. Sahr³¹, W.M. Sang²⁵, E.K.G. Sarkisyan²², C. Sbarra²⁶, A.D. Schaile³¹, O. Schaile³¹,
 P. Scharff-Hansen⁸, S. Schmitt¹¹, A. Schöning⁸, M. Schröder⁸, M. Schumacher²⁵, C. Schwick⁸,
 W.G. Scott²⁰, R. Seuster^{14,h}, T.G. Shears⁸, B.C. Shen⁴, C.H. Shepherd-Themistocleous⁵,
 P. Sherwood¹⁵, G.P. Siroli², A. Skuja¹⁷, A.M. Smith⁸, G.A. Snow¹⁷, R. Sobie²⁶,
 S. Söldner-Rembold^{10,e}, S. Spagnolo²⁰, M. Sproston²⁰, A. Stahl³, K. Stephens¹⁶, K. Stoll¹⁰, D. Strom¹⁹,
 R. Ströhmer³¹, B. Surov⁸, S.D. Talbot¹, S. Tarem²¹, R.J. Taylor¹⁵, R. Teuscher⁹, M. Thiergen¹⁰,
 J. Thomas¹⁵, M.A. Thomson⁸, E. Torrence⁸, S. Towers⁶, T. Trefzger³¹, I. Trigger⁸, Z. Trócsányi^{30,g},
 E. Tsur²², M.F. Turner-Watson¹, I. Ueda²³, R. Van Kooten¹², P. Vannerem¹⁰, M. Verzocchi⁸, H. Voss³,
 D. Waller⁶, C.P. Ward⁵, D.R. Ward⁵, P.M. Watkins¹, A.T. Watson¹, N.K. Watson¹, P.S. Wells⁸,
 T. Wengler⁸, N. Wermes³, D. Wetterling¹¹, J.S. White⁶, G.W. Wilson¹⁶, J.A. Wilson¹, T.R. Wyatt¹⁶,
 S. Yamashita²³, V. Zacek¹⁸, D. Zer-Zion⁸

- ¹School of Physics and Astronomy, University of Birmingham, Birmingham B15 2TT, UK
- ²Dipartimento di Fisica dell' Università di Bologna and INFN, I-40126 Bologna, Italy
- ³Physikalisches Institut, Universität Bonn, D-53115 Bonn, Germany
- ⁴Department of Physics, University of California, Riverside CA 92521, USA
- ⁵Cavendish Laboratory, Cambridge CB3 0HE, UK
- ⁶Ottawa-Carleton Institute for Physics, Department of Physics, Carleton University, Ottawa, Ontario K1S 5B6, Canada
- ⁷Centre for Research in Particle Physics, Carleton University, Ottawa, Ontario K1S 5B6, Canada
- ⁸CERN, European Organisation for Particle Physics, CH-1211 Geneva 23, Switzerland
- ⁹Enrico Fermi Institute and Department of Physics, University of Chicago, Chicago IL 60637, USA
- ¹⁰Fakultät für Physik, Albert Ludwigs Universität, D-79104 Freiburg, Germany
- ¹¹Physikalisches Institut, Universität Heidelberg, D-69120 Heidelberg, Germany
- ¹²Indiana University, Department of Physics, Swain Hall West 117, Bloomington IN 47405, USA
- ¹³Queen Mary and Westfield College, University of London, London E1 4NS, UK
- ¹⁴Technische Hochschule Aachen, III Physikalisches Institut, Sommerfeldstrasse 26-28, D-52056 Aachen, Germany
- ¹⁵University College London, London WC1E 6BT, UK
- ¹⁶Department of Physics, Schuster Laboratory, The University, Manchester M13 9PL, UK
- ¹⁷Department of Physics, University of Maryland, College Park, MD 20742, USA
- ¹⁸Laboratoire de Physique Nucléaire, Université de Montréal, Montréal, Quebec H3C 3J7, Canada
- ¹⁹University of Oregon, Department of Physics, Eugene OR 97403, USA
- ²⁰CLRC Rutherford Appleton Laboratory, Chilton, Didcot, Oxfordshire OX11 0QX, UK
- ²¹Department of Physics, Technion-Israel Institute of Technology, Haifa 32000, Israel
- ²²Department of Physics and Astronomy, Tel Aviv University, Tel Aviv 69978, Israel
- ²³International Centre for Elementary Particle Physics and Department of Physics, University of Tokyo, Tokyo 113-0033, and Kobe University, Kobe 657-8501, Japan
- ²⁴Particle Physics Department, Weizmann Institute of Science, Rehovot 76100, Israel
- ²⁵Universität Hamburg/DESY, II Institut für Experimental Physik, Notkestrasse 85, D-22607 Hamburg, Germany
- ²⁶University of Victoria, Department of Physics, P O Box 3055, Victoria BC V8W 3P6, Canada
- ²⁷University of British Columbia, Department of Physics, Vancouver BC V6T 1Z1, Canada
- ²⁸University of Alberta, Department of Physics, Edmonton AB T6G 2J1, Canada
- ²⁹Research Institute for Particle and Nuclear Physics, H-1525 Budapest, P O Box 49, Hungary
- ³⁰Institute of Nuclear Research, H-4001 Debrecen, P O Box 51, Hungary
- ³¹Ludwigs-Maximilians-Universität München, Sektion Physik, Am Coulombwall 1, D-85748 Garching, Germany

^a and at TRIUMF, Vancouver, Canada V6T 2A3

^b and Royal Society University Research Fellow

^c and Institute of Nuclear Research, Debrecen, Hungary

^d and University of Mining and Metallurgy, Cracow

^e and Heisenberg Fellow

^f now at Yale University, Dept of Physics, New Haven, USA

^g and Department of Experimental Physics, Lajos Kossuth University, Debrecen, Hungary

^h and MPI München

ⁱ now at MPI für Physik, 80805 München.

1 Introduction

Within the framework of the Standard Model of electroweak interactions, the elements of the Cabibbo-Kobayashi-Maskawa mixing matrix are free parameters, constrained only by the requirement that the matrix be unitary. The values of the matrix elements can only be determined by experiment. Heavy Quark Effective Theory (HQET) provides a means to extract the magnitude of the element V_{cb} from particular semileptonic b decays, with relatively small theoretical uncertainties [1].

In this paper, the value of $|V_{cb}|$ is extracted by studying the decay rate for the process $\bar{B}^0 \rightarrow D^{*+} \ell^- \bar{\nu}$ as a function of the recoil kinematics of the D^{*+} meson¹ [2–4]. The decay rate is parameterised as a function of the variable ω , defined as the scalar product of the four-velocities of the D^{*+} and \bar{B}^0 mesons. This is related to the square of the four-momentum transfer from the \bar{B}^0 to the $\ell^- \bar{\nu}$ system, q^2 , by

$$\omega = \frac{m_{D^{*+}}^2 + m_{\bar{B}^0}^2 - q^2}{2m_{\bar{B}^0}m_{D^{*+}}}, \quad (1)$$

and ranges from 1, when the D^{*+} is produced at rest in the \bar{B}^0 rest frame, to about 1.50. Using HQET, the differential partial width for this decay is given by

$$\frac{d\Gamma(\bar{B}^0 \rightarrow D^{*+} \ell^- \bar{\nu})}{d\omega} = \frac{1}{\tau_{\bar{B}^0}} \frac{d\text{Br}(\bar{B}^0 \rightarrow D^{*+} \ell^- \bar{\nu})}{d\omega} = \mathcal{K}(\omega) \mathcal{F}^2(\omega) |V_{cb}|^2, \quad (2)$$

where $\mathcal{K}(\omega)$ is a known phase space term and $\mathcal{F}(\omega)$ is the hadronic form factor for this decay [3]. Although the shape of this form factor is not known, its magnitude at zero recoil, $\omega = 1$, can be estimated using HQET. In the heavy quark limit ($m_b \rightarrow \infty$), $\mathcal{F}(\omega)$ coincides with the Isgur-Wise function [4] which is normalised to unity at the point of zero recoil. Corrections to $\mathcal{F}(1)$ have been calculated to take into account the effects of finite quark masses and QCD corrections, yielding the value and theoretical uncertainty $\mathcal{F}(1) = 0.913 \pm 0.042$ [5]. Since the phase space factor $\mathcal{K}(\omega)$ tends to zero as $\omega \rightarrow 1$, the decay rate vanishes at $\omega = 1$ and the accuracy of the extrapolation relies on achieving a reasonably constant reconstruction efficiency in the region near $\omega = 1$.

Previous measurements of $|V_{cb}|$ have been made using B mesons produced on the $\Upsilon(4S)$ resonance [6] and in Z^0 decays [7–9]. These analyses used a linear or constrained quadratic expansion of $\mathcal{F}(\omega)$ around $\omega = 1$. An improved theoretical analysis, based on dispersive bounds and including higher order corrections, has since become available [10]. This results in a parameterisation for $\mathcal{F}(\omega)$ in terms of $\mathcal{F}(1)$ and a single unknown parameter ρ^2 constrained to lie in the range $-0.14 < \rho^2 < 1.54$, ρ^2 corresponding to the slope of $\mathcal{F}(\omega)$ at zero recoil.

The previous OPAL measurement [9] used the decay chain $D^{*+} \rightarrow D^0 \pi^+$, with the D^0 meson being reconstructed in the exclusive decay channels $D^0 \rightarrow K^- \pi^+$ and $D^0 \rightarrow K^- \pi^+ \pi^0$. In this paper, a new analysis is described in which only the π^+ from the D^{*+} decay is identified, and no attempt is made to reconstruct the D^0 decay exclusively. This technique, first employed by DELPHI [8, 11], gives a much larger sample of $\bar{B}^0 \rightarrow D^{*+} \ell^- \bar{\nu}$ decays than the previous measurement, but also larger background, requiring a rather more complex analysis. The measurement of [9] is also updated to use the new parameterisation of $\mathcal{F}(\omega)$ [10], and improved background models and physics inputs. In both cases, the initial number of B^0 mesons is determined from other measurements of B^0 production in Z^0 decays.

The new reconstruction technique is described in Section 2, the determination of ω for each event in Section 3, the fit to extract $\mathcal{F}(1)|V_{cb}|$ and ρ^2 in Section 4 and the systematic errors in Section 5. The updated exclusive measurement is discussed in Section 6 and the measurements are combined and conclusions drawn in Section 7.

¹Charge conjugate reactions are always implied, and the symbol ℓ refers to either an electron or muon.

2 Inclusive reconstruction of $\bar{B}^0 \rightarrow D^{*+} \ell^- \bar{\nu}$ events

The OPAL detector is well described elsewhere [12]. The data sample used in this analysis consists of about 4 million hadronic Z^0 decays collected during the period 1991–1995, at centre-of-mass energies in the vicinity of the Z^0 resonance. Corresponding simulated event samples were generated using JETSET 7.4 [13] as described in [14].

Hadronic Z^0 decays were selected using standard criteria [14]. To ensure the event was well contained within the acceptance of the detector, the thrust axis direction² was required to satisfy $|\cos \theta_T| < 0.9$. Charged tracks and electromagnetic calorimeter clusters with no associated tracks were then combined into jets using a cone algorithm [15], with a cone half angle of 0.65 rad and a minimum jet energy of 5 GeV. The transverse momentum p_t of each track was defined relative to the axis of the jet containing it, where the jet axis was calculated including the momentum of the track. A total of 3 117 544 events passed the event selection.

The reconstruction of $\bar{B}^0 \rightarrow D^{*+} \ell^- \bar{\nu}$ events was then performed by combining high p and p_t lepton (electron or muon) candidates with oppositely charged pions from the $D^{*+} \rightarrow D^0 \pi^+$ decay. Electrons were identified and photon conversions rejected using neural network algorithms [14], and muons were identified as in [16]. Both electrons and muons were required to have momenta $p > 2$ GeV, transverse momenta with respect to the jet axis $p_t > 0.7$ GeV, and to lie in the polar angle region $|\cos \theta| < 0.9$.

The event sample was further enhanced in semileptonic b decays by requiring a separated secondary vertex with decay length significance $L/\sigma_L > 2$ in any jet of the event. The vertex reconstruction algorithm and decay length significance calculation are described fully in [14]. Together with the lepton selection, these requirements result in a sample which is about 90 % pure in $b\bar{b}$ events.

An attempt was made to estimate the D^0 direction in each jet containing a lepton candidate. Each track (apart from the lepton) and calorimeter cluster in the jet was assigned a weight corresponding to the estimated probability that it came from the D^0 decay. The track weight was calculated from an artificial neural network, trained to separate tracks from b decays and fragmentation tracks in b jets [14]. The network inputs are the track momentum, transverse momentum with respect to the jet axis, and impact parameter significances with respect to the reconstructed primary and secondary vertices (if existing). The cluster weights were calculated using their energies and angles with respect to the jet axis alone, the energies first being corrected by subtracting the energy of any charged tracks associated to the cluster [17].

Beginning with the track or cluster with the largest weight, tracks and clusters were then grouped together until the invariant mass of the group (assigning tracks the pion mass and clusters zero mass) exceeded the charm hadron mass, taken to be 1.8 GeV. If the final invariant mass exceeded 2.3 GeV, the jet was rejected, since Monte Carlo studies showed such high mass D^0 candidates were primarily background. For surviving jets, the momentum \mathbf{p}_{D^0} of the group was used as an estimate of the D^0 direction, giving RMS angular resolutions of about 45 mrad in ϕ and θ . The D^0 energy was calculated as $E_{D^0} = \sqrt{p_{D^0}^2 + m_{D^0}^2}$.

The selection of pions from D^{*+} decays relies on the small mass difference of only 145 MeV [18] between the D^{*+} and D^0 , which means the pions have very little transverse momentum with respect to the D^0 direction. Each track in the jet (other than the lepton) was considered as a slow pion candidate, provided it satisfied $0.5 < p < 2.5$ GeV and had a transverse momentum with respect to the D^0 direction of less than 0.3 GeV. If the pion under consideration was included in the reconstructed D^0 , it was removed and the D^0 momentum and energy recalculated. The final selection was made using the reconstructed mass difference Δm between D^{*+} and D^0 mesons, calculated as

$$\Delta m = \sqrt{E_{D^*}^2 - |\mathbf{p}_{D^*}|^2} - m_{D^0},$$

where the D^{*+} energy is given by $E_{D^*} = E_{D^0} + E_\pi$ and momentum by $\mathbf{p}_{D^*} = \mathbf{p}_{D^0} + \mathbf{p}_\pi$.

²A right handed coordinate system is used, with positive z along the electron beam direction and x pointing to the centre of the LEP ring. The polar and azimuthal angles are denoted by θ and ϕ .

A new secondary vertex was then iteratively reconstructed around an initial seed vertex formed by the intersection of the lepton and slow pion tracks. Every other track in the jet was added in turn to the seed vertex, and the vertex refitted. The track resulting in the lowest vertex fit χ^2 was retained in the seed vertex for the next iteration. The procedure was repeated until no more tracks could be added without reducing the vertex fit χ^2 probability to less than 1%. The decay length L' between the primary vertex and this secondary vertex, and the associated error $\sigma_{L'}$, were calculated as in [14]. The pion candidate was accepted if the decay length satisfied $-0.1 \text{ cm} < L' < 2 \text{ cm}$ and the decay length significance satisfied $L'/\sigma_{L'} > -2$.

The resulting distributions of Δm for opposite and same sign lepton-pion combinations are shown in Figure 1(a) and (b). The predictions of the Monte Carlo simulation are also shown, broken down into contributions from signal $\bar{B}^0 \rightarrow D^{*+} \ell^- \bar{\nu}$ events, ‘resonant’ background containing real leptons and slow pions from D^{*+} decay, and combinatorial background, made up of events with fake slow pions, fake leptons or both.

In Monte Carlo simulation, about 45% of opposite sign events with $\Delta m < 0.17 \text{ GeV}$ are signal $\bar{B}^0 \rightarrow D^{*+} \ell^- \bar{\nu}$ events, 14% are resonant background and 41% are combinatorial background. The resonant background is made up mainly of $B^- \rightarrow D^{*+} \pi^- \ell^- \bar{\nu}$, $\bar{B}^0 \rightarrow D^{*+} \pi^0 \ell^- \bar{\nu}$ and $\bar{B}_s \rightarrow D^{*+} K^0 \ell^- \bar{\nu}$ decays. These are expected to be dominated by b semileptonic decays involving orbitally excited charm mesons (generically referred to as D^{**}), *e.g.* $B^- \rightarrow D^{**0} \ell^- \bar{\nu}$ followed by $D^{**0} \rightarrow D^{*+} \pi^-$. These decays will be denoted collectively by $\bar{B} \rightarrow D^{*+} h \ell^- \bar{\nu}$. Small contributions are also expected from $b \rightarrow D^{*+} \tau \bar{\nu} X$ decays with the τ decaying leptonically, and $b \rightarrow D^{*+} D_s^- X$ with the D_s^- decaying semileptonically (each about 1% of opposite sign events). For same sign events with $\Delta m < 0.17 \text{ GeV}$, there is a small resonant contribution of about 6% from events with a real $D^{*+} \rightarrow D^0 \pi^+$ where the D^0 decays semileptonically, and the rest is combinatorial background.

The most important background, from $\bar{B} \rightarrow D^{*+} h \ell^- \bar{\nu}$ decays, comes from both charged B^+ and neutral B^0 and B_s decays, whereas the signal comes only from B^0 decays. Therefore the charge Q_{vtx} of the reconstructed secondary vertex containing the lepton and slow pion and its estimated error $\sigma_{Q_{\text{vtx}}}$ were calculated, using

$$Q_{\text{vtx}} = \sum_i w_i q_i ,$$

$$\sigma_{Q_{\text{vtx}}}^2 = \sum_i w_i (1 - w_i) q_i^2 ,$$

where w_i is the weight for track i of charge q_i to come from the secondary vertex, and the sums are taken over all tracks in the jet [19,20]. The weights were calculated in a similar way to those used for the D^0 direction reconstruction, using a neural network with the track momentum, transverse momentum and impact parameter significances with respect to the reconstructed primary and secondary vertices as inputs. The weights for the lepton and slow pion candidate tracks were set to one. The vertex charge distributions for opposite sign events with $\Delta m < 0.17 \text{ GeV}$ are shown in Figure 1(c) and (d).

The reconstructed vertex charge and error were used to divide the data into different classes enhanced or depleted in B^+ decays, thus reducing the effect of this background and increasing the statistical sensitivity. Three classes c were used—class 1 where the charge is measured poorly ($\sigma_{Q_{\text{vtx}}} > 0.9$), class 2 where the charge is measured well and is compatible with a neutral vertex ($\sigma_{Q_{\text{vtx}}} < 0.9$, $|Q_{\text{vtx}}| < 0.5$) and class 3 where the charge is measured well and is compatible with a charged vertex ($\sigma_{Q_{\text{vtx}}} < 0.9$, $|Q_{\text{vtx}}| > 0.5$).

3 Reconstruction of ω

The recoil variable ω was estimated in each event using the reconstructed four-momentum transfer to the $\ell \bar{\nu}$ system:

$$q^2 = (E_{B^0} - E_{D^{*+}})^2 - (\mathbf{p}_{B^0} - \mathbf{p}_{D^{*+}})^2$$

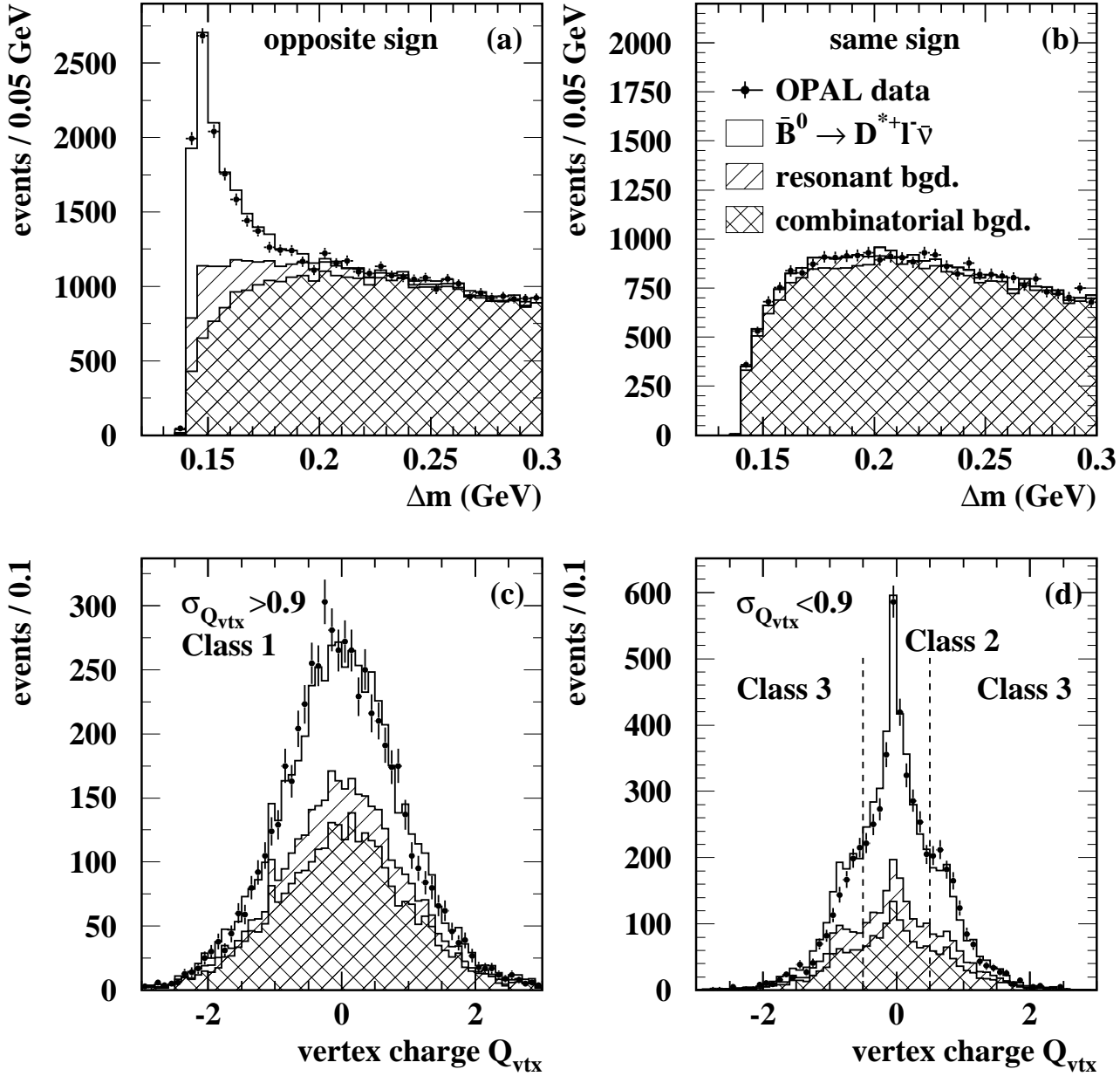


Figure 1: Reconstructed Δm distributions for selected (a) opposite sign and (b) same sign lepton-pion combinations; reconstructed vertex charge Q_{vtx} distributions for opposite sign events with $\Delta m < 0.17 \text{ GeV}$ and (c) $\sigma_{Q_{\text{vtx}}} > 0.9$ and (d) $\sigma_{Q_{\text{vtx}}} < 0.9$. In each case the data are shown by the points with error bars, and the Monte Carlo simulation contributions from signal $\bar{B}^0 \rightarrow D^{*+} \ell^- \bar{\nu}$ decays, other resonant D^{*+} decays and combinatorial background are shown by the open, single and cross hatched histograms respectively. The vertex charge classes 1 (poorly reconstructed), 2 (well reconstructed neutral vertex) and 3 (well reconstructed charged vertex) are indicated.

together with equation 1. The B^0 and D^{*+} energies E_{B^0} and E_{D^*} were estimated directly, whilst the momentum vectors \mathbf{p}_{B^0} and \mathbf{p}_{D^*} were estimated using the energies together with the reconstructed polar and azimuthal angles, as described in more detail below.

Since the slow pion has very little momentum in the rest frame of the decaying D^{*+} , the momentum (and hence energy) of the D^{*+} was estimated by scaling the reconstructed slow pion momentum by $m_{D^{*+}}/m_\pi$, as for the $D^0 \rightarrow K^- \pi^+ \pi^0$ channel in [9]. A small correction (never exceeding 12%) was applied, as a function of $\cos \theta^*$, the angle of the slow pion in the rest frame of the D^0 . This procedure gave a fractional D^{*+} energy resolution of 15%. The polar and azimuthal angles of the D^{*+} were reconstructed using weighted averages of the slow pion and D^0 directions, giving resolutions of about 22 mrad on both ϕ and θ .

The energy of the B^0 was estimated using a technique similar to that described in [21], exploiting the overall energy and momentum conservation in the event to calculate the energy of the unreconstructed neutrino. First, the energy E_{bjet} of the jet containing the B^0 was inferred from the measured particles in the rest of the event, by treating the event as a two-body decay of a Z^0 into a b jet (whose mass was approximated by the B^0 mass) and another object making up the rest of the event. Then, the total fragmentation energy E_{frag} in the b jet was estimated from the measured visible energy in the b jet and the identified B^0 decay products: $E_{\text{frag}} = E_{\text{vis}} - E_\ell - E_{D^*}$. Finally, the B^0 energy was calculated as $E_{B^0} = E_{\text{bjet}} - E_{\text{frag}}$, giving an RMS resolution of 4.4 GeV.

The b direction was estimated using a combination of two techniques. In the first, the momentum vector of the B^0 was reconstructed from its decay products:

$$\mathbf{p}_{B^0} = \mathbf{p}_{D^*} + \mathbf{p}_\ell + \mathbf{p}_{\bar{\nu}},$$

the neutrino energy being estimated from the reverse of the event visible momentum vector: $\mathbf{p}_{\bar{\nu}} = -\mathbf{p}_{\text{vis}}$. The visible momentum was calculated using all the reconstructed tracks and clusters in the event, with a correction for charged particles measured both in the tracking detectors and calorimeters [17]. This direction estimate is strongly degraded if a second neutrino is present (*e.g.* from another semileptonic b decay in the opposite hemisphere of the event), and its error was parameterised as a function of the visible energy in the opposite hemisphere. The resulting resolution is typically between 40 and 100 mrad for both ϕ and θ .

The second method of estimating the B^0 direction used the vertex flight direction—*i.e.* the direction of the vector between the primary vertex and the secondary vertex reconstructed around the lepton and slow pion as described in Section 2. The accuracy of this estimate is strongly dependent on the B^0 decay length, and was used only if the decay length significance $L/\sigma_{L'}$ exceeded 3. After this cut, the angular resolution varies between about 15 and 100 mrad, and is worse for θ in the 1991 and 1992 data where accurate z information from the silicon microvertex detector was not available. The $\bar{B}^0 \rightarrow D^{*+} \ell^- \bar{\nu}$ candidate was rejected if the two reconstruction methods gave θ or ϕ angles disagreeing by more than three standard deviations, which happened in 7% of Monte Carlo signal events. Finally, the two B^0 direction estimates were combined according to their estimated uncertainties, giving average resolutions of 35 mrad on ϕ and 43 mrad on θ , including events where only the first method was used.

The estimate of q^2 derived from the B^0 and D^{*+} energies and angles was improved by applying the constraint that the mass μ of the neutrino produced in the $\bar{B}^0 \rightarrow D^{*+} \ell^- \bar{\nu}$ decay should be zero. The neutrino mass is given from the reconstructed quantities by:

$$\mu^2 = (E_{B^0} - E_{D^*} - E_\ell)^2 - (\mathbf{p}_{B^0} - \mathbf{p}_{D^*} - \mathbf{p}_\ell)^2.$$

The constraint was implemented by calculating q^2 using a kinematic fit, incorporating the measured values and estimated uncertainties of the B^0 and D^{*+} energies and angles (the B^0 angular uncertainties varying event by event). This procedure improved the average q^2 resolution from 2.78 GeV² to 2.57 GeV². In Monte Carlo simulation, 11% of signal events were reconstructed with $q^2 < 0$, corresponding to an unphysical value of ω larger than $\omega_{\text{max}} \approx 1.5$, and were rejected.

The resulting distributions of reconstructed ω for various ranges of true ω (denoted ω') in simulated $\bar{B}^0 \rightarrow D^{*+}\ell^-\bar{\nu}$ decays are shown in Figure 2(a–e). The average RMS ω resolution is about 0.12, but there are significant non-Gaussian tails. The resolution was parameterised (separately for the 1991–2 and 1993–5 data) as a continuous function $R(\omega, \omega')$ giving the expected distribution of reconstructed ω for each true value ω' . The resolution function was implemented as the sum of two asymmetric Gaussians (*i.e.* with different widths either side of the peak) whose parameters were allowed to vary as a function of ω' . The convolution of this resolution function with the Monte Carlo ω' distribution is also shown in Figure 2(a–e), demonstrating that the resolution function models the ω distributions well.

The efficiency to reconstruct $\bar{B}^0 \rightarrow D^{*+}\ell^-\bar{\nu}$ decays $\epsilon(\omega')$ is shown in Figure 2(f), together with a second order polynomial parameterisation. The efficiency varies with ω' , but is reasonably flat in the critical region near $\omega' = 1$ where the extrapolation to measure $\mathcal{F}(1)|V_{cb}|$ is carried out.

4 Fit and results

The values of $\mathcal{F}(1)|V_{cb}|$ and ρ^2 were extracted using an extended maximum likelihood fit to the reconstructed mass difference Δm , recoil ω and vertex charge class c of each event. Both opposite and same sign events with $\Delta m < 0.3 \text{ GeV}$ and $\omega < \omega_{\max}$ were used in the fit, the high Δm and same sign events serving to constrain the combinatorial background normalisation and shapes in the opposite sign low Δm region populated by the $\bar{B}^0 \rightarrow D^{*+}\ell^-\bar{\nu}$ decays. Using the Δm value from each event in the fit, rather than just dividing the data into low Δm ‘signal’ and high Δm ‘sideband’ mass regions, increases the statistical sensitivity as the signal purity varies considerably within the low Δm region.

The logarithm of the overall likelihood was given by

$$\ln \mathcal{L} = \sum_{i=1}^{M^a} \ln \mathcal{L}_i^a + \sum_{j=1}^{M^b} \ln \mathcal{L}_j^b - N^a - N^b \quad (3)$$

where the sums of individual event log-likelihoods $\ln \mathcal{L}_i^a$ and $\ln \mathcal{L}_j^b$ are taken over all the observed M^a opposite sign and M^b same sign events in the data sample, and N^a and N^b are the corresponding expected numbers of events.

The likelihood for each opposite sign event was given in terms of different types or sources of event by

$$\mathcal{L}_i^a(\Delta m_i, \omega_i, c_i) = \sum_{s=1}^4 N_s^a f_{s,c_i}^a M_{s,c_i}(\Delta m_i) P_s(\omega_i) \quad (4)$$

where N_s^a is the number of expected events for source s , $f_{s,c}^a$ is the fraction of events in source s appearing in vertex charge class c , $M_{s,c}(\Delta m)$ is the mass difference distribution for source s in class c and $P_s(\omega)$ the recoil distribution for source s . For each source, the vertex charge fractions $f_{s,c}^a$ sum to one and the mass difference $M_{s,c}(\Delta m_i)$ and recoil $P_s(\omega)$ distributions are normalised to one. The total number of expected events is given by the sum of the individual contributions: $N^a = \sum_{s=1}^4 N_s^a$.

There are four opposite sign sources: (1) signal $\bar{B}^0 \rightarrow D^{*+}\ell^-\bar{\nu}$ events, (2) $\bar{B} \rightarrow D^{*+}h\ell^-\bar{\nu}$ events where the D^{*+} is produced via an intermediate resonance (D^{**}), (3) other opposite sign background involving a genuine lepton and a slow pion from D^{*+} decay and (4) combinatorial background. The sum of sources 2 and 3 are shown as ‘resonant background’ in Figure 1. A similar expression to equation 4 was used for \mathcal{L}_j^b , the event likelihood for same sign events. In this case, only sources 3 and 4 contribute.

The mass difference distributions $M_{c,s}(\Delta m)$ for sources 1–3 were represented by analytic functions, whose parameters were determined using large numbers of simulated events, as were the recoil distributions $P_s(\omega)$ for sources 2 and 3. The fractions in each vertex charge class for sources 1–3 were also taken from simulation. For the signal (source 1), the product of the expected number of events N_1^a

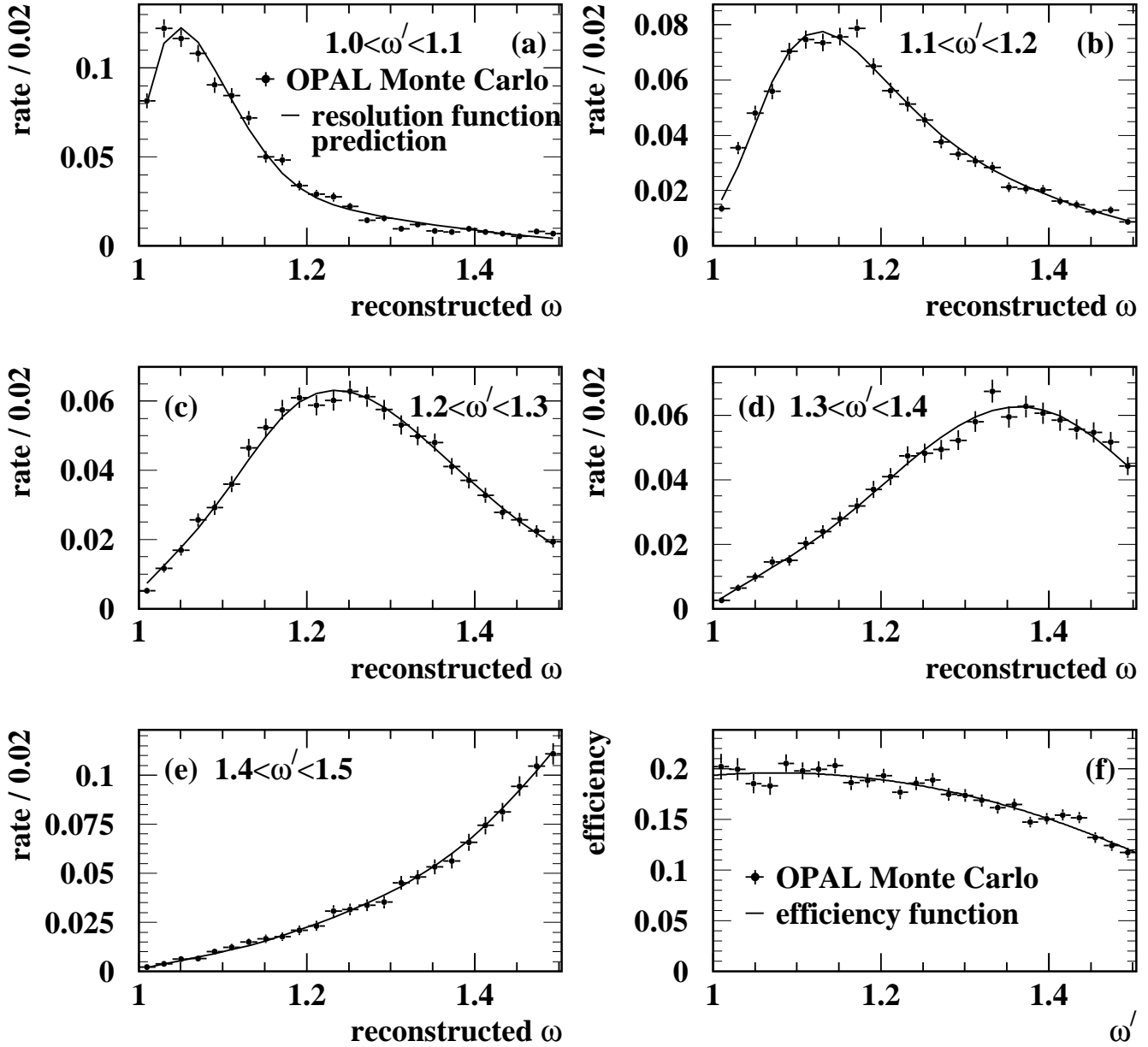


Figure 2: Reconstructed ω distributions for various ranges of true ω' in Monte Carlo $\bar{B}^0 \rightarrow D^{*+} \ell^- \bar{\nu}$ events, together with the prediction from the resolution function. Events reconstructed in the unphysical region with $\omega > \omega_{\max}$ are rejected. The reconstruction efficiency as a function of true ω is also shown.

Quantity	Assumed value	Reference
R_b	$(21.70 \pm 0.09) \%$	[18]
f_{B^0}	$(39.7^{+1.8}_{-2.2}) \%$	[18]
τ_{B^0}	1.56 ± 0.04 ps	[18]
$\text{Br}(D^{*+} \rightarrow D^0 \pi^+)$	$(68.3 \pm 1.4) \%$	[18]
$\text{Br}(b \rightarrow D^{*+} h \ell \bar{\nu})$	$(0.76 \pm 0.16) \%$	[22], see text
$\text{Br}(b \rightarrow D^{*+} \tau^- \bar{\nu} X)$	$(0.65 \pm 0.13) \%$	[18], see text
$\text{Br}(\bar{B}^0 \rightarrow D^{*+} D_s^{(*)-})$	$(4.2 \pm 1.5) \%$	[18]
$\text{Br}(b \rightarrow D^{*+} X)$	$(17.3 \pm 2.0) \%$	[24]
$\text{Br}(c \rightarrow D^{*+} X)$	$(22.2 \pm 2.0) \%$	[24]
$\text{Br}(D^0 \rightarrow K^- \pi^+)$	$(3.85 \pm 0.09) \%$	[18]
$\text{Br}(D^0 \rightarrow K^- \pi^+ \pi^0)$	$(13.9 \pm 0.9) \%$	[18]

Table 1: Input quantities used in the fits for $\mathcal{F}(1)|V_{cb}|$ and ρ^2 . The values marked ‘see text’ are derived using methods explained in Section 4.

and recoil distribution $P_1(\omega)$ was given by convolving the differential partial decay width (equation 2) with the signal resolution function and reconstruction efficiency:

$$N_1^a P_1(\omega) = 4N_Z R_b f_{B^0} \tau_{B^0} \text{Br}(D^{*+} \rightarrow D^0 \pi^+) \int_1^{\omega_{\max}} \mathcal{F}^2(\omega') |V_{cb}|^2 \mathcal{K}(\omega') \epsilon(\omega') R(\omega, \omega') d\omega'$$

where N_Z is the number of hadronic Z^0 decays passing the event selection, $R_b \equiv \Gamma_{b\bar{b}}/\Gamma_{\text{had}}$ is the fraction of hadronic Z^0 decays to $b\bar{b}$, f_{B^0} the fraction of b quarks hadronising to a \bar{B}^0 and τ_{B^0} the B^0 lifetime. The factor of four accounts for the two b hadrons produced per $Z^0 \rightarrow b\bar{b}$ event and the two identified lepton species (electrons and muons). The form factor $\mathcal{F}(\omega')$ is given in [10] in terms of the normalisation $\mathcal{F}(1)$ and slope parameter ρ^2 . The efficiency function $\epsilon(\omega')$ and resolution function $R(\omega, \omega')$ were described in Section 3, and the known phase space factor $\mathcal{K}(\omega')$ is given in [9]. The assumed values of the numerical quantities are given in Table 1.

Since the data are divided into different vertex charge classes enhanced and depleted in B^+ decays, the fit gives some information on the amount of $\bar{B} \rightarrow D^{*+} h \ell^- \bar{\nu}$ background. The predicted level of this background in the fit was therefore allowed to vary under a Gaussian constraint corresponding to the branching ratio of $\text{Br}(b \rightarrow D^{*+} h \ell \bar{\nu}) = (0.76 \pm 0.16) \%$. The latter has been calculated from the measured branching ratio $\text{Br}(b \rightarrow D^{*+} \pi^- \ell \bar{\nu} X) = (0.473 \pm 0.095) \%$ [22], assuming isospin and SU(3) flavour symmetry to obtain the corresponding $b \rightarrow D^{*+} \pi^0 \ell \bar{\nu}$ and $b \rightarrow D^{*+} K^0 \ell \bar{\nu}$ branching ratios. A scaling factor of 0.75 ± 0.25 was included for the last branching ratio to account for possible SU(3) violation effects reducing the branching ratio $D_s^{*+} \rightarrow D^{*+} K^0$ compared to the expectation of $\frac{3}{2} \text{Br}(D_s^{*+} \rightarrow D^{*+} \pi^0)$. The $P_2(\omega)$ distribution for these events was taken from simulation, using the calculation of Leibovich et al. [23] to predict their recoil spectrum.

The numbers $N_3^{a,b}$ and $P_3(\omega)$ distributions for the small background contributions covered by source 3 (both opposite and same sign) were taken from Monte Carlo simulation, with branching ratios adjusted to the values given in Table 1. The branching ratio for $b \rightarrow D^{*+} \tau^- \bar{\nu}$ was derived using the inclusive branching ratio $\text{Br}(b \rightarrow \tau X) = (2.6 \pm 0.4) \%$ [18], assuming a D^{*+} is produced in a fraction 0.25 ± 0.03 of the time, as seen for the corresponding decays $b \rightarrow D^{*+} \ell X$ and $b \rightarrow \ell X$ ($\ell = e, \mu$) [18]. The rate of $b \rightarrow D^{*+} D_s^- X$ was assumed to be dominated by the two body decay $\bar{B}^0 \rightarrow D^{*+} D_s^{(*)-}$. The rate of real D^{*+} decays in the same sign background depends on the production fractions of D^{*+} in $b\bar{b}$ and $c\bar{c}$ events, which were taken from [24].

The parameters of the analytic functions describing the combinatorial background ($N_4^a, N_4^b, f_{4,c}^a, f_{4,c}^b, M_{4,c}(\Delta m)$ and $P_4(\omega)$) were fitted entirely from the data, with only the choice of functional forms motivated by simulation. The shapes of the mass and recoil functions (including a small correlation between Δm and ω) are constrained by the same sign sample (which is almost entirely combinatorial

background), and are the same for each vertex charge class c . The opposite sign high Δm region serves to normalise the number of combinatorial background events in the low Δm region for each vertex charge class.

The values of $\mathcal{F}(1)|V_{cb}|$ and ρ^2 were extracted by maximising the total likelihood given by equation 3. The values of $\mathcal{F}(1)|V_{cb}|$ and ρ^2 were allowed to vary, together with the level of $\bar{B} \rightarrow D^{*+} h \ell^- \bar{\nu}$ background and 13 auxiliary parameters describing the combinatorial background distributions. A result of

$$\begin{aligned}\mathcal{F}(1)|V_{cb}| &= (37.5 \pm 1.2) \times 10^{-3}, \\ \rho^2 &= 1.12 \pm 0.14\end{aligned}$$

was obtained, where the errors are only statistical. The correlation between $\mathcal{F}(1)|V_{cb}|$ and ρ^2 is 0.77. The distributions of reconstructed ω for opposite and same sign events with $\Delta m < 0.17$ GeV, together with the fit results, are shown in Figure 3. The fit describes the data well, both in this region and the high Δm region dominated by combinatorial background, for all three of the vertex charge classes.

By integrating the differential partial decay width (equation 2) over all values of ω , the branching ratio $\text{Br}(\bar{B}^0 \rightarrow D^{*+} \ell^- \bar{\nu})$ was also determined to be

$$\text{Br}(\bar{B}^0 \rightarrow D^{*+} \ell^- \bar{\nu}) = (5.92 \pm 0.27) \%,$$

where again the error is statistical only. This result is consistent with the world average once systematic errors are included.

Many previous results have been obtained using a constrained quadratic expansion for the form factor: $\mathcal{F}(\omega) = \mathcal{F}(1) [1 - a^2(\omega - 1) + b(\omega - 1)^2]$, where a is a slope parameter to be determined by the fit, and b is constrained to $b = 0.66a^2 - 0.11$ [25]. To allow comparison with such measurements, the fit was also performed with this parameterisation of $\mathcal{F}(\omega)$, giving the results $\mathcal{F}(1)|V_{cb}| = (36.9 \pm 1.2) \times 10^{-3}$ and $a^2 = 0.88 \pm 0.14$, the correlation between $\mathcal{F}(1)|V_{cb}|$ and a^2 being 0.79. The difference in the two curvature parameters ρ^2 and a^2 is in good agreement with the expectation of $\rho^2 - a^2 \approx 0.21$ [10].

5 Systematic Errors

Systematic errors arise from the uncertainties in the fit input parameters given in Table 1, the Monte Carlo modelling of the signal ω resolution, the recoil spectrum of $b \rightarrow D^{**} \ell \bar{\nu}$ decays and selection efficiencies, and possible biases in the fitting method. The resulting systematic errors on the values of $\mathcal{F}(1)|V_{cb}|$, ρ^2 and $\text{Br}(\bar{B}^0 \rightarrow D^{*+} \ell^- \bar{\nu})$ are summarized in Table 2 and described in more detail below.

Input quantities: The various numerical fit inputs were each varied according to the errors given in Table 1 and the fit repeated to assess the resulting uncertainties.

$b \rightarrow D^{} \ell \bar{\nu}$ decays:** The calculation of Leibovich et al. [23] was used to simulate the recoil spectrum of $\bar{B} \rightarrow D^{*+} h \ell^- \bar{\nu}$ decays, assumed to be produced via the semileptonic decay $B^0 \rightarrow D^{**} \ell \bar{\nu}$. Here D^{**} represents a P-wave orbitally excited charm meson. The calculation predicts the recoil spectra and relative rates of semileptonic decays involving both the narrow D_1 and D_2^* states and wide D_0^* and D_1^* states. All these decays are suppressed close to $\omega = 1$ by an extra factor of $(\omega^2 - 1)$ when compared with the signal $\bar{B}^0 \rightarrow D^{*+} \ell^- \bar{\nu}$ decays. This reduces the uncertainty due to the rate of $\bar{B} \rightarrow D^{*+} h \ell^- \bar{\nu}$ decays in the extrapolation of the signal recoil spectrum to $\omega = 1$. Non-resonant $\bar{B} \rightarrow D^{*+} h \ell^- \bar{\nu}$ decays are not included in the model, but are not expected to contribute close to $\omega = 1$.

The differential decay rates in [23] are given in terms of five possible expansion schemes and several unknown parameters: a kinetic energy term η_{ke} and the slopes of the Isgur-Wise functions for the narrow and wide D^{**} states $\hat{\tau}_1$ and $\hat{\zeta}_1$. These parameters were varied within the allowed

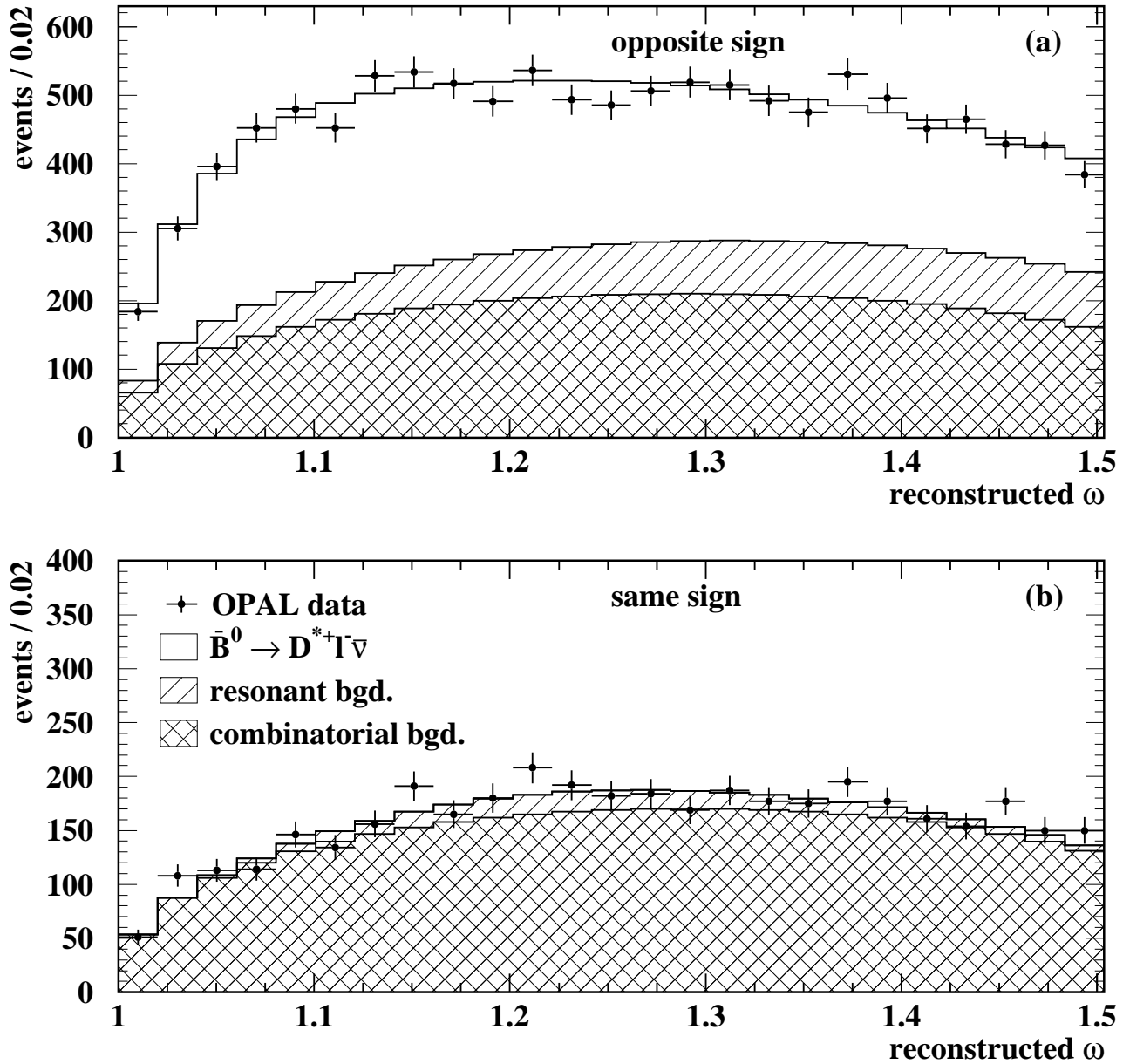


Figure 3: Distributions of reconstructed ω for (a) opposite sign and (b) same sign events with $\Delta m < 0.17$ GeV. The data are shown by the points with error bars and the expectation from the fit result by the histograms. The contributions from signal $\bar{B}^0 \rightarrow D^{*+} \ell^- \bar{\nu}$, resonant and combinatorial backgrounds are indicated.

Error Source	$\Delta(\mathcal{F}(1) V_{cb})/(\mathcal{F}(1) V_{cb})$ (%)	$\Delta\rho^2$	$\Delta\text{Br}/\text{Br}$ (%)
R_b value	0.2	-	0.4
B^0 lifetime	1.3	-	2.6
f_{B^0} value	+2.8 -2.3	-	+5.5 -4.5
$\text{Br}(D^{*+} \rightarrow D^0\pi^+)$	1.0	-	2.1
$\text{Br}(b \rightarrow D^{*+}\tau^-\bar{\nu})$	0.1	0.00	0.4
$\text{Br}(b \rightarrow D^{*+}D_s^{(*)-})$	0.3	0.01	1.3
$\text{Br}(b \rightarrow D^{*+}X)$	0.0	0.00	0.1
$\text{Br}(c \rightarrow D^{*+}X)$	0.0	0.00	0.0
$b \rightarrow D^{**}\ell\bar{\nu}X$ rate	0.6	0.05	2.9
$b \rightarrow D^{**}\ell\bar{\nu}X$ model	4.1	0.19	3.5
b fragmentation	1.1	0.12	3.2
D^0 decay multiplicity	1.2	0.08	2.2
ω reconstruction	2.2	0.12	2.1
Lepton identification efficiency	1.2	-	2.3
Vertex tag efficiency	1.7	-	3.4
Track reconstruction efficiency	0.1	0.10	4.3
Tracking resolution	2.4	0.04	4.4
Fitting method	1.9	0.05	0.6
Total	6.8	0.29	11.5

Table 2: Summary of systematic errors on the measured values of $\mathcal{F}(1)|V_{cb}|$, ρ^2 and $\text{Br}(\bar{B}^0 \rightarrow D^{*+}\ell^-\bar{\nu})$ for the inclusive analysis. The fractional errors on $\mathcal{F}(1)|V_{cb}|$ and $\text{Br}(\bar{B}^0 \rightarrow D^{*+}\ell^-\bar{\nu})$ are given, whereas the errors on ρ^2 are absolute.

ranges $-0.75 < \eta_{ke} < 0.75$ GeV, $-2 < \hat{\tau}_1 < -1$ and $-2 < \hat{\zeta}_1 < 0$ subject to the constraint that the ratio $R = \Gamma(\bar{B} \rightarrow D_2^*\ell\bar{\nu})/\Gamma(\bar{B} \rightarrow D_1\ell\bar{\nu})$ lie within the measured range $R = 0.37 \pm 0.16$ [22, 26]. This excludes the expansion schemes A_∞ and B_∞ of [23] and constrains the allowable values of η_{ke} in the others. The fraction of $\bar{B} \rightarrow D^{**}\ell^-\bar{\nu}$ decays involving the narrow D_1 and D_2^* states, which is not precisely predicted, was varied in the range 0.22 ± 0.06 , obtained by comparing the measured rates for B^0 semileptonic decays involving D^+ , D^{*+} , D_1 and D_2^* with the inclusive semileptonic decay rate [18, 22, 26]. The systematic errors were determined as half the difference between the two parameter sets giving the most extreme variations in $\mathcal{F}(1)|V_{cb}|$ and ρ^2 , and the central values were adjusted to half way between these two extremes. The values of both $\mathcal{F}(1)|V_{cb}|$ and ρ^2 are most sensitive to variations in η_{ke} , which is constrained by the measured value of R .

b fragmentation: The effect of uncertainties in the average b hadron energy $\langle x_E \rangle = E_b/E_{\text{beam}}$ was assessed in Monte Carlo simulation by reweighting the events so as to vary $\langle x_E \rangle$ in the range 0.702 ± 0.008 [28], and repeating the fit. The largest of the variations observed using the fragmentation functions of Peterson, Collins and Spiller, Kartvelishvili and the Lund group [27] were taken as systematic errors.

D^0 decay multiplicities: The signal reconstruction efficiency and vertex charge distributions are sensitive to the B^0 decay multiplicity, which depends only on the D^0 decay for the B^0 decay channels of interest. The systematic error was assessed by varying separately the D^0 charged and π^0 decay multiplicities in Monte Carlo simulation according to the measurements of Mark III [29]. The branching ratio $D^0 \rightarrow K^0, \bar{K}^0$ was also varied according to its uncertainty [18]. The resulting uncertainties on $\mathcal{F}(1)|V_{cb}|$ and ρ^2 from each variation were added in quadrature to determine the total systematic errors.

ω reconstruction: The modelling of the ω resolution depends on the description of the D^{*+} and B^0 energy and angular distributions in the simulation. The reconstructed D^{*+} and B^0 energy distributions in data and simulation were compared, and the means were found to differ by 0.04 and 0.13 GeV respectively. The opposite hemisphere missing energy was found to agree within 5%. The corresponding systematics were assessed by shifting or scaling the data distributions and repeating the ω reconstruction and fit. The modelling of the angular resolution was checked by studying the agreement of the two angular estimators—the slow pion and D^0 directions for the D^{*+} , and the missing energy vector and vertex flight directions for the B^0 . The angular resolutions were found to be up to 5% worse in data, and the systematic error was assessed by degrading the simulated resolution appropriately. Finally, the fraction of events with ω reconstructed in the physical region ($\omega < \omega_{\max}$) was found to be 3.5% smaller in the data, in both opposite and same sign charge samples. The reconstruction efficiency was corrected for this effect, and an additional systematic error of half the correction (1.7%) assumed. The final systematic errors due to ω resolution modelling are dominated by the B^0 θ resolution.

Lepton identification efficiency: The electron identification efficiency has been studied using control samples of pure electrons from $e^+e^- \rightarrow e^+e^-$ events and photon conversions, and found to be modelled to a precision of 4.1% [14]. The muon identification efficiency has been studied using muon pairs produced in two-photon collisions and $Z^0 \rightarrow \mu^+\mu^-$ events, giving an uncertainty of 2.1% [30].

Vertex tag efficiency: The fraction of hemispheres with identified leptons which also had a selected secondary vertex was found to be about 4% less in data than in simulation. The overall fraction of vertex tagged hemispheres was also found to be about 4% lower in data. These discrepancies were translated into systematic errors on the efficiency to tag a semileptonic b decay with a secondary vertex in either the same or the opposite hemisphere, in each case attributing the whole discrepancy to a mismodelling of b hadron decays. The resulting errors on the same and opposite hemisphere tagging efficiencies were taken to be fully correlated.

Track reconstruction efficiency: The overall track reconstruction efficiency is known to be modelled to a precision of 1% [14], and a similar uncertainty was found to be appropriate for the particular class of slow pion tracks from D^{*+} decays. The systematic error was assessed by randomly removing 1% of tracks in the simulation and repeating the fit.

Tracking resolution: Uncertainties in the tracking detector resolution affect the efficiency, ω reconstruction and vertex charge distributions. The associated error was assessed in the simulation by applying a global 10% degradation to all tracks, independently in the r - ϕ and r - z planes, as in [14].

Fit method: The entire fitting procedure was tested on a fully simulated Monte Carlo sample seven times bigger than the data, with true values of $\mathcal{F}(1)|V_{cb}| = 32.5 \times 10^{-3}$ and $\rho^2 = 1.3$. The fit gave the results $\mathcal{F}(1)|V_{cb}| = (31.8 \pm 0.5) \times 10^{-3}$ and $\rho^2 = 1.25 \pm 0.07$, consistent with the true values. For each variable, the larger of the deviation of the result from the true value and the statistical error were taken as a systematic errors due to possible biases in the fit. Additionally, the large Monte Carlo sample was reweighted to change the values of $\mathcal{F}(1)|V_{cb}|$ and ρ^2 , and the fit correctly recovered the modified values. To verify the correctness of the statistical errors returned by the fit, it was performed on many separate subsamples, and the distribution of fitted results studied. Further checks on the data included performing the analysis separately for B^0 decays involving electrons and muons, dividing the sample according to the year of data taking, and varying the lepton transverse momentum cut. In all cases, consistent results were obtained.

Including all systematic uncertainties, the final result of the inclusive analysis is

$$\mathcal{F}(1)|V_{cb}| = (37.5 \pm 1.2 \pm 2.5) \times 10^{-3},$$

$$\rho^2 = 1.12 \pm 0.14 \pm 0.29,$$

where the first error is statistical and the second systematic in each case.

6 Measurement using exclusively reconstructed D^{*+} decays

In this analysis, the D^0 from the $\bar{B}^0 \rightarrow D^{*+}\ell^{-}\bar{\nu}$, $D^{*+} \rightarrow D^0\pi^+$ decay is reconstructed exclusively in the decay modes $D^0 \rightarrow K^-\pi^+$ (‘3-prong’) and $D^0 \rightarrow K^-\pi^+\pi^0$ (‘satellite’—where the π^0 is not reconstructed). The event selection, reconstruction and determination of ω are exactly the same as described in [9]. The determination of the signal and background fractions, and the fit to extract $\mathcal{F}(1)|V_{cb}|$ and ρ^2 are performed as in [9], but have been updated using the improved form factor parameterisation [10], the updated input parameters given in Table 1 and the $b \rightarrow D^{**}\ell\bar{\nu}$ decay model [23] discussed in Section 5.

The fit is performed on 814 3-prong and 1396 satellite candidates, of which 505 ± 44 and 754 ± 72 are attributed to $\bar{B}^0 \rightarrow D^{*+}\ell^{-}\bar{\nu}$ signal decays. The result of the fit is

$$\begin{aligned} \mathcal{F}(1)|V_{cb}| &= (36.8 \pm 1.6 \pm 2.0) \times 10^{-3}, \\ \rho^2 &= 1.31 \pm 0.21 \pm 0.16, \end{aligned}$$

where again the first errors are statistical and the second systematic. The statistical correlation between $\mathcal{F}(1)|V_{cb}|$ and ρ^2 is 0.95. The distribution of reconstructed ω for selected candidates (both 3-prong and satellite) is shown in Figure 4. The branching ratio $\text{Br}(\bar{B}^0 \rightarrow D^{*+}\ell^{-}\bar{\nu})$ has also been determined to be

$$\text{Br}(\bar{B}^0 \rightarrow D^{*+}\ell^{-}\bar{\nu}) = (5.11 \pm 0.19 \pm 0.49) \%$$

The systematic errors arise from uncertainties in the background levels in the selected samples, as well as uncertainties in the Monte Carlo simulations. They have been evaluated following the procedures described in [9], and are summarised in Table 3. The selection efficiency error includes contributions from lepton identification efficiency, b fragmentation and detector resolution uncertainties, described in detail in [31]. The largest change with respect to the previous result is due to the improved $b \rightarrow D^{**}\ell\bar{\nu}$ modelling, with the suppression of this background at values of ω close to one. This reduces the statistical error, the systematic uncertainty due to the rate of such decays, and shifts the central value of $\mathcal{F}(1)|V_{cb}|$ upwards as compared to [9].

7 Conclusions

The CKM matrix element $|V_{cb}|$ has been measured by studying the rate of the semileptonic decay $\bar{B}^0 \rightarrow D^{*+}\ell^{-}\bar{\nu}$ as a function of the recoil kinematics of both inclusively and exclusively reconstructed D^{*+} mesons. The two results are combined, taking into account the statistical correlation of 18% and correlated systematic errors from physics inputs and detector resolution. The results are:

$$\begin{aligned} \mathcal{F}(1)|V_{cb}| &= (37.1 \pm 1.0 \pm 2.0) \times 10^{-3}, \\ \rho^2 &= 1.21 \pm 0.12 \pm 0.20, \\ \text{Br}(\bar{B}^0 \rightarrow D^{*+}\ell^{-}\bar{\nu}) &= (5.26 \pm 0.20 \pm 0.46) \%, \end{aligned}$$

where the first result is statistical and the second systematic in each case. The statistical and systematic correlations between $\mathcal{F}(1)|V_{cb}|$ and ρ^2 are 0.90 and 0.54 respectively. These results supersede our previous publication [9]. They are consistent with other determinations of $\mathcal{F}(1)|V_{cb}|$ at LEP [7, 8] and the $\Upsilon(4S)$ resonance [6]. The branching ratio is consistent with the world average result of $(4.60 \pm 0.27) \%$ [18]. The result for $\mathcal{F}(1)|V_{cb}|$ is the most precise to date from any single experiment.

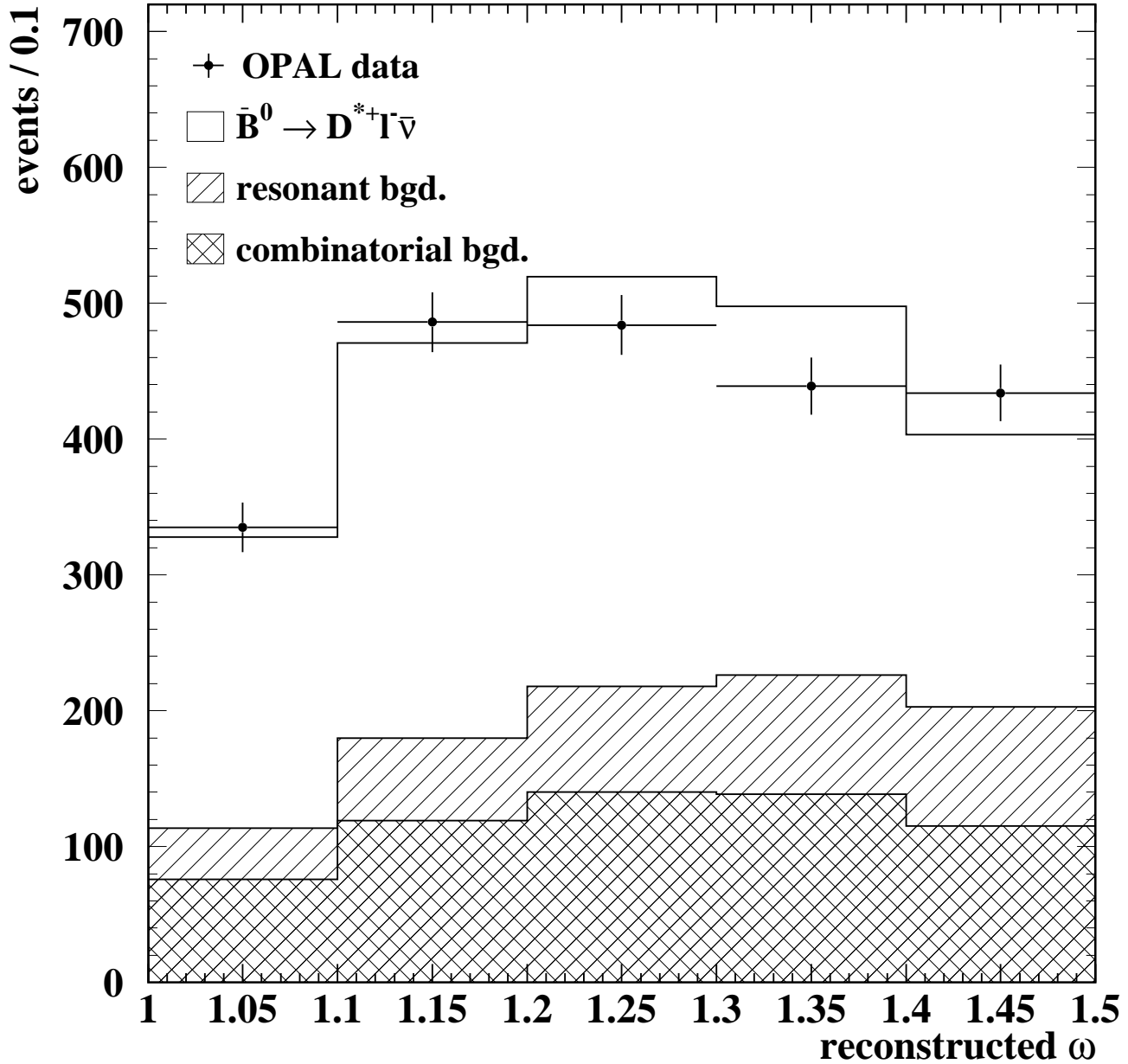


Figure 4: Distribution of reconstructed ω for $\bar{B}^0 \rightarrow D^{*+} \ell^- \bar{\nu}$ candidates in the exclusive analysis. The data are shown by the points with statistical error bars, and the fit result by the histogram. The contributions from signal $\bar{B}^0 \rightarrow D^{*+} \ell^- \bar{\nu}$, resonant and combinatorial backgrounds are indicated.

Error Source	$\Delta(\mathcal{F}(1) V_{cb})/(\mathcal{F}(1) V_{cb})$ (%)	$\Delta\rho^2$	$\Delta\text{Br}/\text{Br}$ (%)
R_b value	0.2	-	0.4
B^0 lifetime	1.2	-	2.4
f_{B^0} value	2.5	-	4.9
$\text{Br}(D^{*+} \rightarrow D^0\pi^+)$	1.0	-	2.0
$\text{Br}(D^0 \rightarrow K^-\pi^+)$	0.4	0.011	0.2
$\text{Br}(D^0 \rightarrow K^-\pi^+\pi^0)$	2.6	0.025	3.8
$\text{Br}(b \rightarrow D^{*+}\tau^-\bar{\nu})$	0.1	-	0.2
$\text{Br}(b \rightarrow D^{*+}D_s^{(*)-})$	0.2	-	0.4
$b \rightarrow D^{**}\ell\bar{\nu}X$ rate	1.1	0.078	2.0
$b \rightarrow D^{**}\ell\bar{\nu}X$ model	1.0	0.128	5.0
Combinatorial background	1.2	0.012	1.7
Fake leptons	0.2	-	0.4
Fake D^0	0.5	0.005	0.7
ω reconstruction	1.4	0.035	-
Selection efficiency	2.9	0.005	3.1
Total	5.5	0.157	9.5

Table 3: Summary of systematic errors on the measured values of $\mathcal{F}(1)|V_{cb}|$, ρ^2 and $\text{Br}(\bar{B}^0 \rightarrow D^{*+}\ell^-\bar{\nu})$ for the exclusive analysis. The fractional errors on $\mathcal{F}(1)|V_{cb}|$ and $\text{Br}(\bar{B}^0 \rightarrow D^{*+}\ell^-\bar{\nu})$ are given, whereas the errors on ρ^2 are absolute.

Using the theoretical estimate $\mathcal{F}(1) = 0.913 \pm 0.042$ [5], the value of $|V_{cb}|$ is determined to be

$$|V_{cb}| = (40.7 \pm 1.1 \pm 2.2 \pm 1.6) \times 10^{-3},$$

where the uncertainties are statistical, systematic and theoretical respectively.

Acknowledgements

We particularly wish to thank the SL Division for the efficient operation of the LEP accelerator at all energies and for their continuing close cooperation with our experimental group. We thank our colleagues from CEA, DAPNIA/SPP, CE-Saclay for their efforts over the years on the time-of-flight and trigger systems which we continue to use. In addition to the support staff at our own institutions we are pleased to acknowledge the

Department of Energy, USA,

National Science Foundation, USA,

Particle Physics and Astronomy Research Council, UK,

Natural Sciences and Engineering Research Council, Canada,

Israel Science Foundation, administered by the Israel Academy of Science and Humanities,

Minerva Gesellschaft,

Benoziyo Center for High Energy Physics,

Japanese Ministry of Education, Science and Culture (the Monbusho) and a grant under the Monbusho International Science Research Program,

Japanese Society for the Promotion of Science (JSPS),

German Israeli Bi-national Science Foundation (GIF),

Bundesministerium für Bildung, Wissenschaft, Forschung und Technologie, Germany,

National Research Council of Canada,

Research Corporation, USA,

Hungarian Foundation for Scientific Research, OTKA T-029328, T023793 and OTKA F-023259.

References

- [1] See for example, M. Neubert, Phys. Rep. 245 (1994) 259;
M. Neubert, Int. J. Mod. Phys. A. C11 (1996) 4173.
- [2] M.A. Shifman and M.B. Voloshin, Sov. J. Nucl. Phys. 47 (1988) 511.
- [3] M. Neubert, Phys. Lett. B264 (1991) 455;
M. Neubert, Phys. Lett. B338 (1994) 84.
- [4] N. Isgur and M. Wise, Phys. Lett. B232 (1989) 113;
N. Isgur and M. Wise, Phys. Lett. B237 (1990) 527;
A.F. Falk, H. Georgi, B. Grinstein and M.B. Wise, Nucl. Phys. B343 (1990) 1.
- [5] The BaBar Physics Book, ed. P.F. Harrison and H.R. Quinn, SLAC-R-054, October 1998, and references therein.
- [6] ARGUS collaboration, H. Albrecht et al., Z. Phys. C57 (1993) 533;
CLEO collaboration, B. Barish et al., Phys. Rev. D51 (1995) 1014;
CLEO collaboration, M. Athanas et al., Phys. Rev. Lett. 79 (1997) 2208;
CLEO collaboration, J. Bartelt et al., Phys. Rev. Lett. 82 (1999) 3746.
- [7] ALEPH collaboration, D. Buskulic et al., Phys. Lett. B395 (1997) 373.
- [8] DELPHI collaboration, P. Abreu et al., Z. Phys. C71 (1996) 539.
- [9] OPAL collaboration, K. Ackerstaff et al., Phys. Lett. B395 (1997) 128.
- [10] I. Caprini, L. Lellouch and M. Neubert, Nucl. Phys. B530 (1998) 153.
- [11] DELPHI collaboration, P. Abreu et al., Z. Phys. C74 (1997) 19.
- [12] OPAL collaboration, K. Ahmet et al., Nucl. Instrum. Methods A305 (1991) 275;
P.P. Allport et al., Nucl. Instrum. Methods A324 (1993) 34;
P.P. Allport et al., Nucl. Instrum. Methods A346 (1994) 476.
- [13] T. Sjöstrand, Comp. Phys. Comm. 82 (1994) 74.
- [14] OPAL collaboration, G. Abbiendi et al., Eur. Phys. J. C8 (1999) 217.
- [15] OPAL collaboration, R. Akers et al., Z. Phys. C63 (1994) 197.
- [16] OPAL collaboration, P.D. Acton et al., Z. Phys. C58 (1993) 523.
- [17] OPAL collaboration, K. Ackerstaff et al., Eur. Phys. J. C2 (1998) 213;
OPAL collaboration, G. Abbiendi et al., ‘Search for Neutral Higgs Bosons in e^+e^- Collisions at $\sqrt{s} = 189\text{ GeV}$ ’, CERN-EP/99-96, accepted by Eur. Phys. J. C.
- [18] Particle Data Group, C. Caso et al., Eur. Phys. J. C3 (1998) 1.
- [19] OPAL collaboration, R. Akers et al., Z. Phys. C66 (1995) 19.
- [20] OPAL collaboration, K. Ackerstaff et al., Eur. Phys. J. C5 (1998) 379.
- [21] OPAL collaboration, R. Akers et al., Z. Phys. C66 (1995) 555.
- [22] ALEPH collaboration, D. Buskulic et al., Z. Phys. C73 (1997) 601.
- [23] A. Leibovich, Z. Ligeti, I. Stewart and M. Wise, Phys. Rev. D57 (1998) 308.

- [24] OPAL collaboration, K. Ackerstaff et al., Eur. Phys. J. C1 (1998) 439.
- [25] M. Neubert, Phys. Lett. B264 (1991) 455;
M. Neubert, Phys. Lett. B338 (1994) 84;
I. Caprini and M. Neubert, Phys. Lett. B380 (1996) 376 and references therein.
- [26] CLEO collaboration, A. Anastassov et al., Phys. Rev. Lett. 80 (1998) 4127.
- [27] C. Peterson, D. Schlatter, I. Schmitt and P. Zerwas, Phys. Rev. D27 (1983) 105;
P. Collins and T. Spiller, J. Phys. G11 (1985) 1289;
V.G. Kartvelishvili, A.K. Likhoded and V.A. Petrov, Phys. Lett. B78 (1978) 615;
B. Anderson, G. Gustafson and B. Söderberg, Z. Phys. C20 (1983) 317.
- [28] The LEP collaborations, ALEPH, DELPHI, L3 and OPAL, Nucl. Instrum. Methods A378 (1996) 101.
Updated averages are described in ‘Presentation of LEP Electroweak Heavy Flavour Results for Summer 1998 Conferences’, LEPHF 98-01 (see <http://www.cern.ch/LEPEWWG/heavy/>).
- [29] MARK III collaboration, D. Coffman et al., Phys. Lett. B263 (1991) 135.
- [30] OPAL collaboration, G. Abbiendi et al., ‘Measurements of inclusive semileptonic branching fractions of b hadrons in Z^0 decays’, CERN-EP/99-78, accepted by Eur. Phys. J. C.
- [31] OPAL collaboration, R. Akers et al., Z. Phys. C67 (1995) 57.